Structural Characterization of Weakly Attached Cross-Bridges in the A·M·ATP State in Permeabilized Rabbit Psoas Muscle

S. Xu, J. Gu, G. Melvin, and L. C. Yu
National Institute of Arthritis, Musculoskeletal and Skin Diseases, National Institutes of Health, Bethesda, Maryland 20892 USA

ABSTRACT It is well established that in a skeletal muscle under relaxing conditions, cross-bridges exist in a mixture of four weak binding states in equilibrium (A·M·ATP, A·M·ADP·P_i, M·ATP, and M·ADP·P_i). It has been shown that these four weak binding states are in the pathway to force generation. In the past their structural, biochemical, and mechanical properties have been characterized as a group. However, it was shown that the myosin heads in the M·ATP state exhibited a disordered distribution along the thick filament, while in the M·ADP·P_i state they were well ordered. It follows that the structures of the weakly attached states of A·M·ATP and A·M·ADP·P_i could well be different. Individual structures of the two attached states could not be assigned because protocol for isolating the two states has not been available until recently. In the present study, muscle fibers are reacted with *N*-phenylmaleimide such that ATP hydrolysis is inhibited, i.e., the cross-bridge population under relaxing conditions is distributed only between the two states of M·ATP and A·M·ATP. Two-dimensional x-ray diffraction was applied to determine the structural characteristics of the attached A·M·ATP state. Because the detached state of M·ATP is disordered and does not contribute to layer line intensities, changes as a result of increasing attachment in the A·M·ATP state are attributable to that state alone. The equilibrium toward the attached state was achieved by lowering the ionic strength. The results show that upon attachment, both the myosin and the first actin associated layer lines increased intensities, while the sixth actin layer line was not significantly affected. However, the intensities remain weak despite substantial attachment. The results, together with modeling (see J. Gu, S. Xu and L. C. Yu, 2002, *Biophys. J.* 82:2123–2133), suggest that there is a wide range of orientation of the attached A·M·ATP cross-bridges while the myosin heads maintain some degree of helical distribution on the thick filament, suggesting a high degree of flexibility in the actomyosin complex. Furthermore, the lack of sensitivity of the sixth actin layer line suggests that the binding site on actin differs from the putative site for rigor binding. The significance of the flexibility in the A·M·ATP complex in the process of force generation is discussed.

INTRODUCTION

One of the challenges in understanding the chemomechanical coupling mechanism of muscle contraction is to determine the structures of myosin and actin associated with each biochemical intermediate state in the ATP hydrolysis cycle (Scheme 1):

$$\begin{array}{ccccccc} \text{M·ATP} & \leftrightarrow & \text{M·ADP·P}_i & \leftrightarrow & \text{M·ADP} & \leftrightarrow & \text{M} \\ \updownarrow & & \updownarrow & & \updownarrow & & \updownarrow \\ \text{A·M·ATP} & \leftrightarrow & \text{A·M·ADP·P}_i & \leftrightarrow & \text{A·M·ADP} & \leftrightarrow & \text{A·M} \end{array}$$

Scheme 1

where M is myosin and A is actin. In recent years, striking advances have been made in our understanding of the relationship between structure and function of the actomyosin interactions. Crystal structures of myosin subfragment 1 (S1) isoforms complexed with various nucleotides have shown several conformations that suggest conformational change as a function of nucleotide state. (Rayment et al., 1993b, 1996; Fisher et al., 1995; Houdusse et al., 2000). Spectroscopic techniques have also shown multiple conformations of S1 depending on the nucleotide bound (Papp et al., 1992; Xiao et al., 1998; Shih et al., 2000). However, structures of the actomyosin interactions have been largely derived from modeling based on electron microscopy, mostly obtained from isolated filaments. In a muscle cell, actomyosin interactions occur within the confines of a filament lattice, where the periodicities of the contractile filaments do not match. It is inevitable that there is a distribution of conformation/orientation within the population of the myosin heads bound to actin. The in vivo structures could well differ from those determined by in vitro techniques. Furthermore, if the actomyosin affinity is weak, a noninvasive technique would be required for preserving the structures. X-ray diffraction studies from skeletal muscle, the technique used in the present study, are noninvasive. In addition, data are obtained from muscle fibers where the contractile apparatus is left basically intact. The results, albeit at relatively low resolution, reveal the distributions and orientations of the myosin heads (cross-bridges) in the filament lattice, and their changes are recorded simultaneously with changes in function.

By applying the x-ray diffraction technique to permeabilized muscle fibers, structures of the detached cross-bridges in the M·ATP, M·ADP· P_i, M·ADP, and M states (Xu et al., 1999b) and those of the rigor state (A·M) and the A·M·ADP state (e.g., Kim et al., 1998) have been studied in detail. Several plausible models for the latter two states, including the active state, now exist (Whittaker et al., 1995; Tsaturyan et al., 1999; Juanhuix et al., 2001). The purpose of the

Submitted January 3, 2001, and accepted for publication January 18, 2002.

Address reprint requests to Dr. Sengen Xu, NIAMS, NIH, Bldg. 50, Rm. 1349, Bethesda, MD 20892-8024. Tel.: 301-594-3333; Fax: 301-402-0009; E-mail: xus@exchange.nih.gov.

0006-3495/02/04/2111/12 $2.00

present study is to characterize the state A·M·ATP as it occurs in muscle cells.

A·M·ATP is one of the four weak binding states (A·M·ATP, A·M·ADP·P_i, M·ATP, and M·ADP·P_i) (Eisenberg and Hill, 1985; Brenner, 1986; Taylor, 1989; Chalovich, 1992), which are characterized by low affinity between actin and myosin (Brenner et al., 1982). They have been shown to be in the pathway to force generation; if the formation of A·M·ATP and/or A·M·ADP·P_i states are blocked, force generation is inhibited (Brenner et al., 1991; Kraft et al., 1995). Because of their physiological significance, clarification of their structures is therefore critical. Previously, we have shown that the distribution of the cross-bridges in the M·ATP state in the thick filament is disordered, while M ·ADP·P_i is well ordered (Xu et al., 1999b). However, one could not yet assign definitive structures to A·M·ADP·P_i and A·M·ATP individually, because a protocol for isolating the two states was not available until recently.

By chemically modifying the SH1 and SH2 groups in the myosin head by the alkylating agent *N*-phenylmaleimide (NPM), the ATP hydrolysis step is inhibited, i.e., in the presence of ATP, NPM-reacted myosin is trapped in the M·ATP and the A·M·ATP states. The binding affinity of the NPM-reacted myosin for actin (Xie et al., 1999) and the stiffness of the muscle fibers (Barnett et al., 1992) have been shown not to be affected significantly by the chemical modification. The x-ray diffraction patterns in the presence of MgATP at low temperature are well matched between the untreated and the treated muscle fibers, with the exception that the intensity of the first myosin layer line is somewhat lower in the treated muscle fibers. Furthermore, the modified myosin remains capable of making a reversible structural transition from the weak to the strong binding states (Xu et al., 1998). These results indicate that the structure of the myosin head is slightly modified by the NPM treatment, but the ADP·P_i states are excluded. Because the M·ATP state makes little contribution to the layer line intensities, any enhancement of the layer lines is thus attributable to a single state of A·M·ATP.

Displacing the equilibrium toward the attached state was achieved by lowering the ionic strength (Brenner et al., 1982). The results show that, unlike the strong attachment, both the myosin and the first actin layer lines increase their intensities, while the sixth layer line is not sensitive to weak attachment. Preliminary results have been reported previously (Xu et al., 1999a).

METHODS

Muscle preparation and solutions

Single bundles of muscle fibers

All experiments were performed on chemically skinned bundles of fibers of rabbit psoas major. Immediately after dissection, muscle strips, ~1 mm in width, were fixed at the two ends, keeping the muscle at resting length. The strips were incubated for 30 min. at 5°C in skinning solution with 0.5% Triton X-100, and then were transferred to skinning solution without the detergent. Single bundles, fasciculi, ~0.3 mm × 0.6 mm in cross-section and ~30 mm in length, were dissected from the larger strip with care (see Xu et al., 1997). A single bundle was mounted in a specimen chamber for x-ray diffraction experiments equipped with a motor for slow, steady stretching. The sarcomere length (SL) of the bundles was adjusted to 2.4–2.5 μm. Some bundles for non-overlap experiments were stretched over a period of 2–4 h to SL = 4.0–4.2 μm, and their sarcomere length was monitored by laser light diffraction during stretch (see Xu et al., 1999b).

Solutions

The following solutions were used for the experiments. 1) Skinning solution (in mM): 5 KH_2PO_4, 5 MgAc, 5 EGTA, 3 Na_2ATP, 50 CrP, 5 NaN_3, 2 DTT, protease inhibitor cocktail from Sigma (St. Louis, MO) (100 mM AEBSF, 4 mM bestatin, 1.4 mM E-64, 2.2 mM leupeptin, 1.5 mM pepstatin A, 80 μM aprotinin), pH 7.0; 2) Relaxing solution contained (in mM): 2 MgATP, 2 $MgCl_2$, 2 EGTA, 5 DTT, 10 imidazole, pH 7.0, ionic strength (μ) = 27 mM. Ionic strength was adjusted by adding 10 mM creatine phosphate and 133 mM potassium propionate for μ = 170 mM, and 10 mM creatine phosphate with 13 mM potassium propionate for μ = 50 mM. To complete the ATP-backup system, ~109 units/ml creatine kinase (CPK) was added in the relaxing solution; 3) Rigor solution contained (in mM): 2.5 EGTA, 2.5 EDTA, 10 imidazole, 5 DTT, 150 potassium propionate, pH 7.0, μ = 170 mM. Before applying the rigor solution the bundles were rinsed several times with a "quick rinse" solution containing (in mM): 5 EGTA, 15 EDTA, 20 imidazole, pH 7.0, μ = 70 mM (Brenner et al., 1991); 4) NPM solution contained (in mM): 0.1 mM NPM, 4 EGTA, 1 $MgCl_2$, 4 MgATP, 125 KCl, 10 imidazole (Xu et al., 1998), pH 7.0.

During the entire course of the experiments, the solution in the chamber was continuously mixed by a push-pull syringe pump at the rate of ~0.5 ml/s to minimize any gradient along the length of the bundles. To reduce radiation damage, the specimen chamber was moved up and down continuously for a length of 6 mm at a constant rate of 4 mm/s by a stepping motor (Aerotech, Pittsburgh, PA).

NPM treatment of fiber bundles

NPM has been shown to be an effective agent for selectively alkylating the SH1 and SH2 of the myosin molecule, both in solution and in muscle fibers (Barnett et al., 1992; Ehrlich et al., 1995). By following the procedure developed by Schoenberg et al., 100% of the two thiol groups are labeled. In the presence of MgATP and at low temperature, the mechanical and structural properties of the cross-bridges in an NPM-reacted muscle fiber closely match those in an untreated fiber (Barnett et al., 1992; Barnett and Schoenberg, 1993; Xu et al., 1998), while the cross-bridges can bind to actin strongly if MgATP is completely washed out (Xu et al., 1998). However, the actin-activated ATPase is suppressed by 20,000-fold, bringing the hydrolysis to a halt (Xie et al., 1999). These results indicate that the myosin head modified by the NPM is an ideal analog state of M·ATP.

In this study, the NPM treatment was carried out according to Barnett et al. (1992) and Xu et al. (1998). The single bundles were reacted with NPM (0.1 mM) solution for 1 h, and the reaction was terminated by replacing the NPM solution with normal relaxing solution containing 5 mM DTT. In a few sets of experiments x-ray diffraction patterns were also recorded before the NPM treatment.

X-ray source, camera, and detector system

The experiments were performed at beamlines X9B (the Regional Center for Time-Resolved Synchrotron Spectroscopy) and X27C (Advanced Poly-

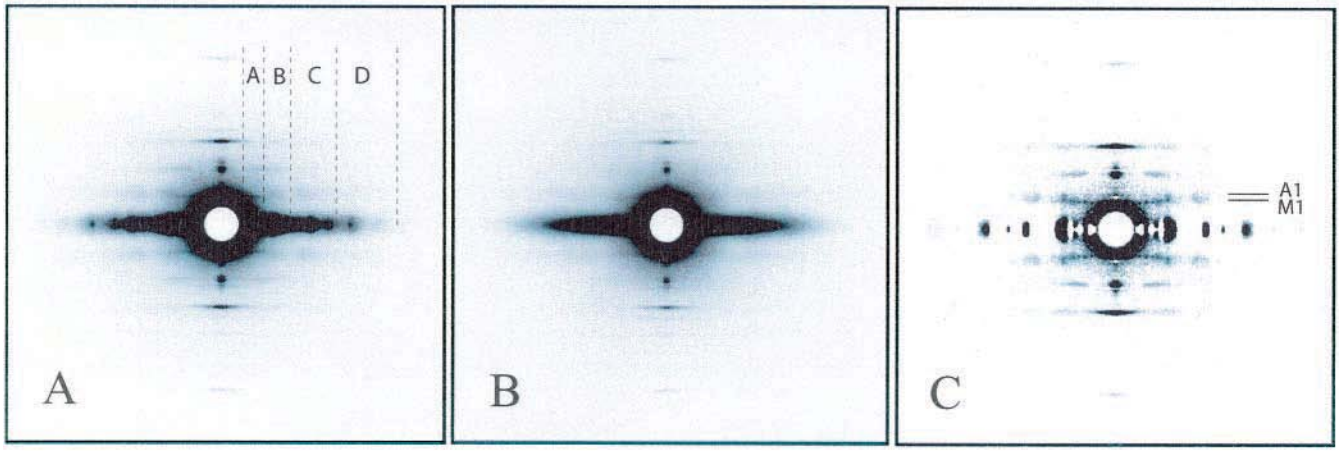

FIGURE 1 X-ray diffraction patterns from a single bundle of skinned rabbit psoas muscle fibers reacted with NPM. Sarcomere length (SL) = 2.4 μm, pH 7.0, T = 5°C. (*A*) In relaxing solution, μ = 27 mM; (*B*) in relaxing solution, μ = 170 mM; (*C*) difference pattern which is pattern A subtracted by pattern B. M1 and A1 indicate the axial positions of the first myosin layer line and the first actin layer line. The difference pattern demonstrates the unique feature of the weak attachment in the A·M·ATP state that *both* the myosin and the actin-based layer lines are enhanced with increasing attachment. The parts that did not change in (*A*) and (*B*) (e.g., the actin filament and some residual myosin-based contributions) do not show in (*C*). The patterns were obtained using the synchrotron radiation beamline X27C of the National Synchrotron Light Source (NSLS) at Brookhaven National Laboratory (BNL), Upton, NY. Exposure time: 2 min. The regions between the vertical dotted lines in pattern A show four vertical slices; their lateral widths are "A," 0.00305–0.00390 Å^{-1} (328–256 Å in real space); "B," 0.00404–0.00543 Å^{-1} (248–184 Å); "C," 0.00610–0.00964 Å^{-1} (164–104 Å); "D," 0.00978–0.01512 Å^{-1} (102–66 Å) (see Data Reduction and Analysis for detail).

mer PRT) at the National Synchrotron Light Source (NSLS), Brookhaven National Laboratory (BNL), Upton, NY. The optics of the Beamline X9B consisted of a double crystal monochromator with a sagittally bent second crystal providing horizontal focusing followed by a dynamically bent, flat mirror providing harmonics rejection and vertical focusing. Si-111 crystals were used as monochromators. The monochromatic x-ray beam was point-focused on the detector but collimated to dimensions of ~0.6 mm horizontal × 0.4 mm vertical at the specimen. The size of the focal spot was 0.43 mm FWHM horizontal and 0.27 mm FWHM vertical. The specimen-to-detector distance was 1500 mm. The optics of X27C uses a double-multilayer (silicon/tungsten) monochromator. A three-pinhole system is used for collimating the monochromatized beam. The beam size at the specimen is ~ 0.4 mm in diameter and specimen-to-detector distance was 1500 mm. A MAR Research CCD detector or imaging plate detector (Hamburg, Germany) with 0.1 mm × 0.1 mm pixel size was used for collecting the x-ray data.

The fiber bundle was held vertically. The exposure time for each pattern was 2 min in general. The maximum accumulated exposure time for each bundle was ≤20 min. In some cases, the solution background patterns were taken at the end of a series of x-ray exposures on each bundle.

To directly compare the intensities with minimum error, diffraction patterns were recorded from the same bundles for all the conditions of interest (e.g., changes of ionic strength and temperature). The spacings of all reflections were calibrated at the beginning of this series of experiments by the 1/144.3 Å^{-1} meridional reflection from skinned rabbit psoas muscle in rigor at μ = 170 mM and T = 20°C (see Xu et al., 1997 for details).

In summary, the experimental protocol included stirring the chamber to avoid solution gradient, scanning the fibers through the beam to minimize local radiation damage, and comparing multiple experimental conditions using the same fiber bundle to ensure the reproducibility of the recorded data.

Data reduction and analysis

The data were displayed and analyzed on a Silicon Graphics Indigo workstation (Mountain View, CA). The data in the four quadrants were first rotated, folded, and averaged. The program made slices parallel to the meridian and to the equator of the diffraction patterns, and summed the intensities within the slices to generate one-dimensional intensity profiles for further analysis. All integrated intensities (I) in the tables were normalized by the integrated intensity of the equatorial reflection [1, 0] obtained from the same NPM-treated bundles in the relaxing solution at μ = 50 mM and 5°C.

Four vertical slices parallel to the meridian were made with the ranges of (A) 0.00305–0.00390 Å^{-1} (328–256 Å in real space), (B) 0.00404–0.00543 Å^{-1} (248–184 Å), (C) 0.00610–0.00964 Å^{-1} (164–104 Å), (D) 0.00978–0.01512 Å^{-1} (102–66 Å) (see Fig. 1 *A*). Within each slice, the background was first subtracted using PCA program (Nucleus, Oak Ridge, TN) by interpolating linearly in the region of maxima (Xu et al., 1997). Intensities above the background were then integrated. In addition, a set of finer vertical cuts with a width of only five pixels was made for the first three layer lines. The purpose was to delineate the mixture of the first and second myosin-based layer lines, the first actin-based layer line, and possibly the troponin-based layer lines (She et al., 1999). The cuts were contiguous and together they covered a wide region in the lateral direction ranging from the meridian to 0.012 Å^{-1} (83 Å in real space). The profiles of these vertical cuts were curve fitted by the Peak Fit program (Jandel Scientific, San Rafael, CA). Then the integrated intensities of the curve-fitted peaks were calculated after subtracting the background fitted by a two-exponential function. The profiles *along* those layer lines in the lateral direction were obtained by pasting together the calculated vertical intensities. For the higher-order myosin-based layer lines (third through sixth) and actin-based layer line (sixth), simple horizontal cuts (parallel to the equator) were made with five pixels in (vertical) width. The final quantitative results were used for modeling (See Gu et al., 2002).

RESULTS

With NPM treatment, the cross-bridges in the relaxing solution are only distributed among the M·ATP and A·M·ATP states (Xie et al., 1999). Equilibrium is shifted toward the

attached state by lowering the ionic strength (Brenner et al., 1982, 1984; McKenna et al., 1989). Based on an effective actin concentration of 1 mM (Brenner et al., 1986; Frisbie et al., 1998) and a binding constant of S1 for actin in the presence of MgATP of $\sim 7 \times 10^3$ M^{-1} at 20 mM ionic strength (Chalovich et al., 1983; Frisbie et al., 1998), one may estimate that at $\mu = 27$ mM the fraction of cross-bridges attached to actin could be as high as 80%, while at $\mu = 170$ mM the fraction is reduced to ~30%.

Fig. 1, *A* and *B* show typical x-ray diffraction patterns from an NPM-reacted fiber bundle in the relaxing solution at 5°C, $\mu = 27$ mM (*A*) and $\mu = 170$ mM (*B*). Pattern (*A*) shows stronger myosin-based layer lines *and* a stronger first actin-based layer line compared to those in (*B*). By curve-fitting, the spacings for the myosin-based first and second layer lines, the actin-based first layer line, and the troponin-based first and second layer lines were determined to be 431.0, 216.5, 361.1, 385.1, and 192.6 Å. The spacings for higher-order myosin layer lines (third to sixth) were respectively centered at 144.3, 108.2, 86.6, and 72.2 Å, and for the sixth actin layer line, at 58.8 Å. Some of the main features of the intensity changes upon lowering the ionic strength are highlighted in the difference pattern (*C*) (pattern (*A*) minus pattern (*B*)). The difference pattern reveals a characteristic feature of the weak attachment: increases in *both* the myosin layer lines and the actin layer lines are clearly visible. Although it may appear that in Fig. 1 *C* the layer lines are separate and distinct, they are still a mixture of the myosin and the actin layer lines, particularly in the inner part of the pattern. The centroid in slice "C" in Fig. 1 *C*, which we have analyzed in the same manner as in Figs. 5 and 6, is at 384 Å (data not shown). The parts that did not change (e.g., the actin filament, and some residual myosin-based contributions) would not appear in Fig. 1 *C*.

Effects of NPM alkylation: a lack of temperature sensitivity in the thick filament.

At low temperature (5°C) and in the presence of MgATP, the diffraction patterns of the untreated muscle fibers and the NPM-treated fibers are well matched. There are, however, some differences between the untreated and the NPM-treated fibers. In the untreated fibers, the first layer line (AMLL1) shows more of a myosin helix component at 430 Å compared with that after the NPM treatment (Fig. 2, *A* and *B*). This component is attributable to the disappearance of the M·ADP·P_i/A·M·ADP·P_i states, which would contribute to the myosin layer lines (Xu et al., 1999b, 2001). Because of the inhibition of hydrolysis, the decrease in the 430 Å component is expected.

The major difference, however, lies in their sensitivity to temperature changes. It was shown that there was a disorder → order transition in the myosin filaments as the temperature is raised from 5°C to above 20°C (Wray, 1987) (Wakabayashi et al., 1988; Xu et al., 1996; Malinchik et al., 1997). The ordering of the helical array of myosin cross-bridges was closely correlated with the transition of the myosin from the M·ATP to the M·ADP·P_i state (Xu et al., 1999b). In the present study, for the NPM-treated muscle fibers the diffraction patterns did not change with temperature, a strong indication that the myosin is trapped in the M·ATP/A·M·ATP states and ATP hydrolysis is fully inhibited. The profiles across the layer lines (in slices A and B) with $\mu = 50$ mM at 5°C and 20°C are shown in Fig. 3, *A* and *B*.

Effects of ionic strength on equatorial reflections

Fig. 4 shows intensity profiles along the equator of the patterns obtained from an NPM-reacted bundle in the relaxing solution, for $\mu = 170$ mM and for $\mu = 27$ mM at 5°C. After the NPM treatment, the intensity ratio I_{11}/I_{10} under relaxing condition at $\mu = 170$ mM increases slightly from 0.62 to 0.74, suggesting that the total number of weakly bound cross-bridges increases slightly. Lowering the ionic strength from $\mu = 170$ mM to 27 mM at 5°C causes an increase in I_{11}/I_{10} from 0.74 to 1.64, indicating a substantial increase in cross-bridge attachment (Fig. 4 and Table 1). The filament lattice spacing decreased from $d_{10} = 424.7$ Å and $d_{11} = 244.8$ Å at $\mu = 170$ mM to $d_{10} = 399.9$ Å and $d_{11} = 229.3$ Å at $\mu = 27$ mM (Table 1). The results closely match the well-established results in untreated relaxed fibers (Brenner and Yu, 1985).

The myosin-based and the actin-based layer lines

In Fig. 1 the intensity of the first layer line becomes stronger with a lowering of the ionic strength. The part of the layer line closest to the meridian, marked as A, shows a larger spacing along the fiber axis than those in the regions marked as B, C, D. We therefore analyzed the profiles in segments.

Four vertical slices A, B, C, D parallel to the meridian were made across the layer lines (Fig. 1). Fig. 5 *A* shows the profiles closest to the meridian (slice A). The centroid in the axial direction of the first layer line (i.e., the first peak) is 432 Å, which indicates that the main contribution originates from the myosin-based helical structure. Six orders of myosin-based layer lines and the sixth actin layer line at 59 Å are also visible in the diffraction patterns (only first layer line is shown in the figure). Fig. 6 *A* shows the profiles in slice B. Its lateral range covers the peak area along the first actin layer line from the actin filaments if they were decorated with strongly bound myosin heads (Huxley and Brown, 1967; Xu et al., 1997). Although the axial centroid is determined to be 406 Å, this part of the layer line consists of a mixture of components (Fig. 6 *A*). The positions of the sub-peaks are ~430, 385, and 365 Å. Based on the spacings, it is

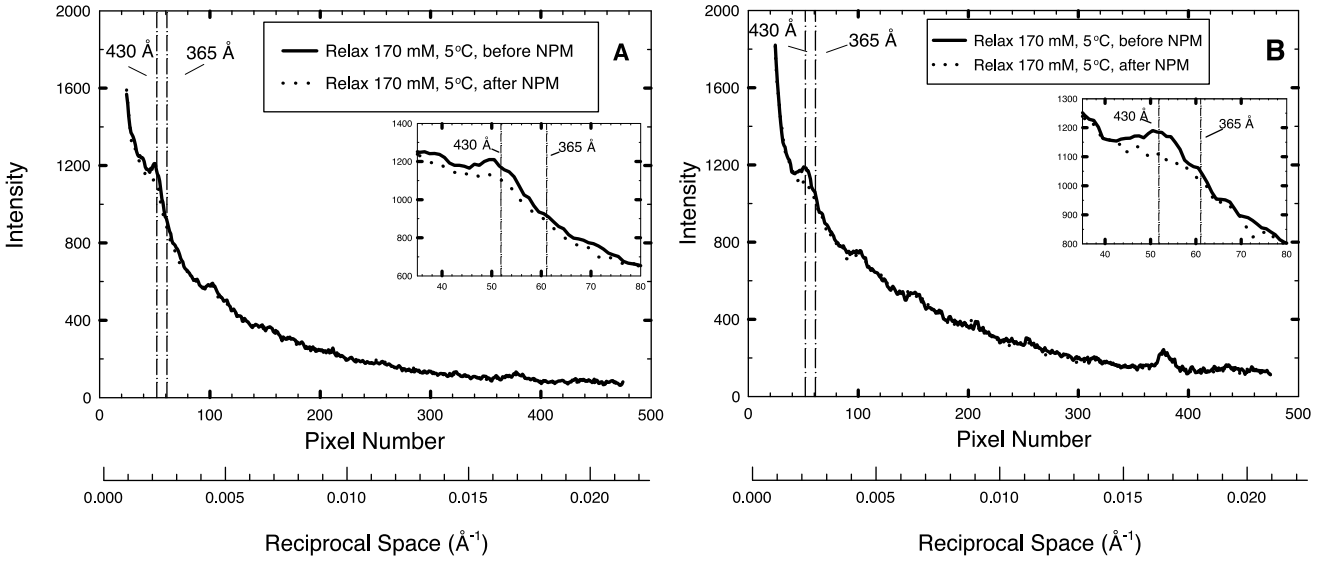

FIGURE 2 NPM treatment does not affect layer line intensities appreciably except the first myosin layer line. (*A*) Comparison of the intensity profiles in the vertical slice "A" (same definition as in Fig. 1) of the x-ray diffraction patterns obtained before (*solid line*) and after (*dotted line*) NPM treatment from a single bundle in relaxing solution at 170 mM and 5°C. (*B*) Profiles from the same diffraction patterns but from slice "B" (same definition as in Fig. 1). Our previous results (Xu et al., 1999b) indicated that at 5°C in untreated fibers ~45% of the myosin heads are in the M·ADP·P_i state, contributing to myosin layer line intensities. Here the low myosin layer line intensity is consistent with reducing M·ADP·P_i essentially to zero and the remaining intensity contributed by M·ATP state.

reasonable to assume that this part of the layer line originates from 1) the myosin helix with a 430 Å repeat; 2) the actin helix with a 365 Å repeat; and probably 3) a helix with a 385 Å repeat. For slices C and D the centroids of the layer lines are 399 and 378 Å (profiles not shown; see Table 2 for spacings), also suggesting the mixtures of components.

The intensity of the first myosin-actin layer line in slice A dominated by myosin helix with ~430 Å increases significantly at lower ionic strength in association

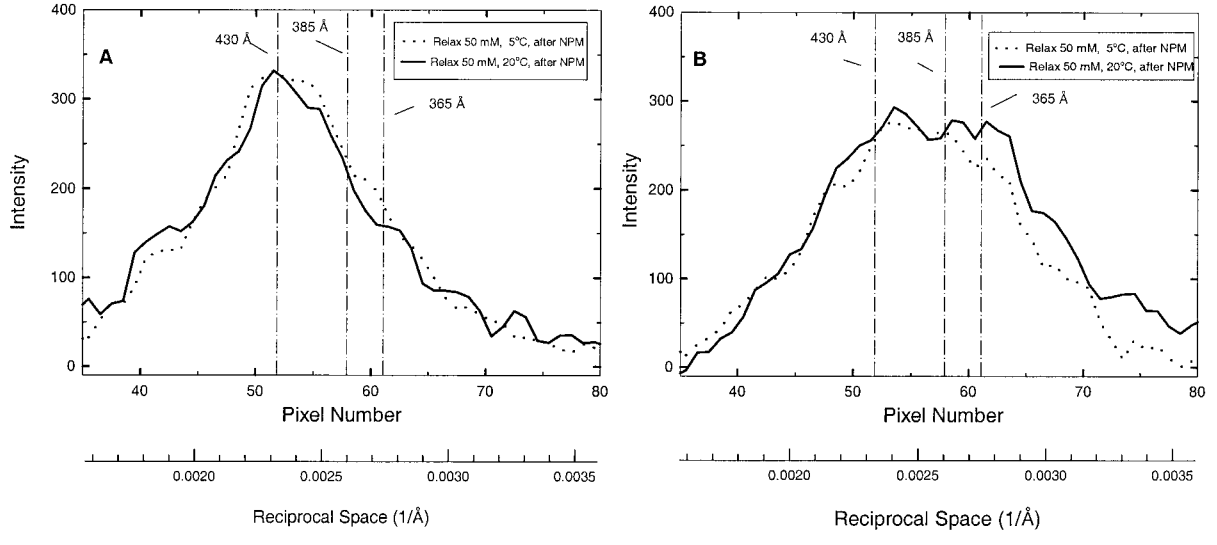

FIGURE 3 Temperature has little effect on the myosin layer lines obtained from an NPM-reacted relaxed bundle. SL = 2.4 μm and μ = 50 mM. The profiles in (*A*) and (*B*) were derived from the vertical slices "A" and "B" as defined in Fig. 1. *Dotted line*, at 5°C; *solid line*, at 20°C. As a contrast, in the unmodified fibers at μ = 170 mM, cooling from 25° to 5°C reduces the first myosin layer line intensity by 75–80%, consistent with the reduction of M·ADP·P_i from ~93% to ~44% (Xu et al., 1999b). The lack of change here indicates that cross-bridges remain in the M·ATP ⇄ A·M·ATP equilibrium regardless of temperature. The profiles only show the overlap region of the myosin-actin layer lines for clarity.

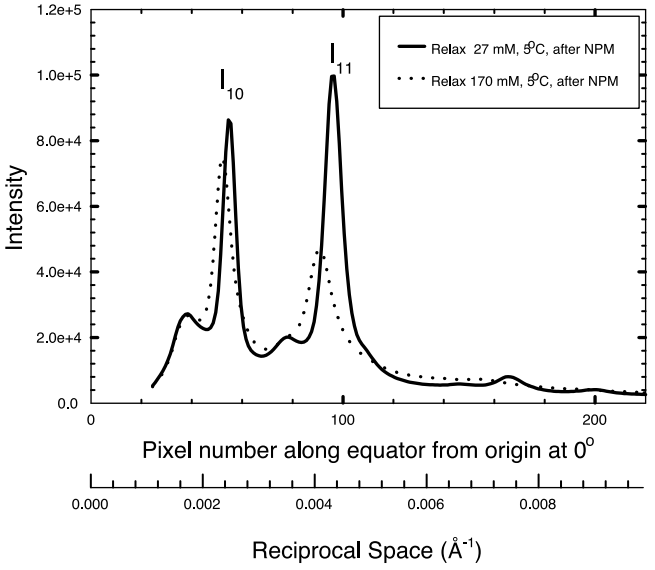

FIGURE 4 Intensity profiles along the equator of the patterns in Fig. 1, *A* and *B* obtained from an NPM-reacted bundle in relaxing solution at 5°C, $\mu = 27$ mM (*solid line*) and $\mu = 170$ mM (*dotted line*). Lowering the ionic strength from 170 to 27 mM causes a significant increase in I_{11}/I_{10}, indicating a substantial increase in cross-bridge attachment.

with the increasing fraction of the weakly bound cross-bridges (Fig. 5 *A*). The intensities of the second and third myosin layer lines in slice A increase as well. The higher orders (fourth through sixth) in this axial profile, however, do not show a measurable increase. As for slice B, the total intensity of the first layer line, which was composed of at least two components of first myosin and first actin layer lines, also increases significantly from $\mu = 170$ to 27 mM (Fig. 6 *A*). The integrated intensities and spacings of the first layer line in the profiles (A, B, C, D) under various conditions are summarized in Table 2.

For modeling the structure of the cross-bridges in the A·M·ATP state, a more detailed delineation of intensity distributions is needed. A set of contiguous vertical cuts with a narrow (five pixel) width was made based on Fig. 1 *A* (see Methods). Fig. 7 shows the reconstructed intensity distribution along the myosin-based and the actin-based layer lines. Some features are revealed more clearly in this representation of the data. It is noted that on the first myosin layer line there are actually two peaks (at 0.0033 $Å^{-1}$ and 0.0069 $Å^{-1}$). The second peak changed to a much lesser extent than the first peak between the low and the high ionic conditions, leaving the difference close to the noise level in the difference pattern of Fig. 1 *C*. Similarly, the fourth and fifth myosin layer lines were almost invisible in the difference pattern. As it turned out, these intensities (the second peak of the first myosin layer line and the fourth and fifth layer lines) contain the information on the whereabouts of the second

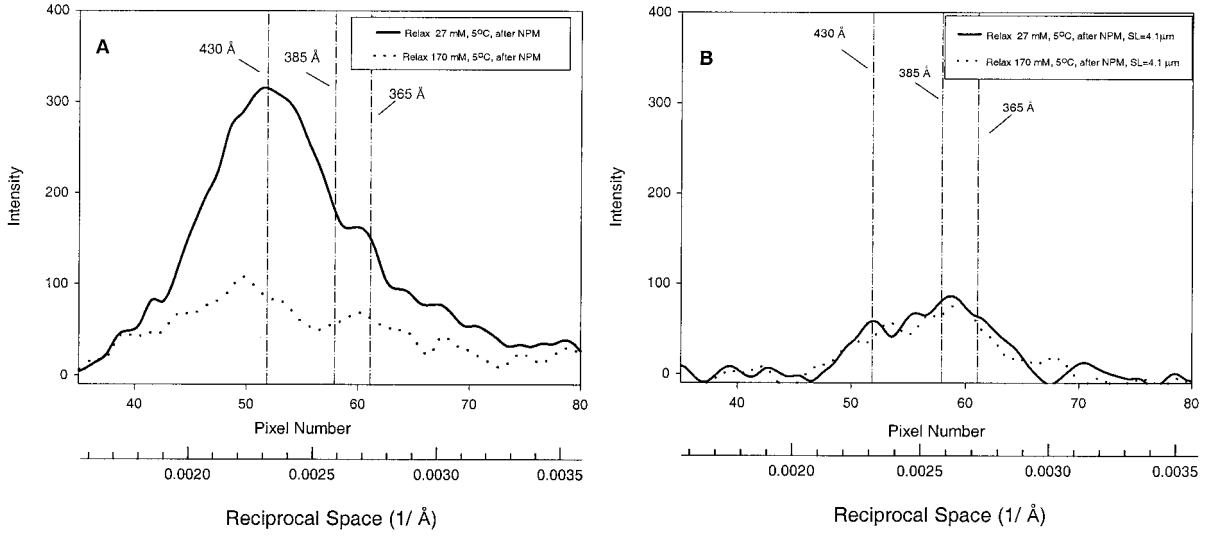

FIGURE 5 Effects of ionic strength on layer line intensities (I). The profiles only show the overlap region of the myosin-actin layer lines for clarity. *Solid lines*, $\mu = 27$ mM; *dotted lines*, $\mu = 170$ mM. (*A*) Intensity profiles based on the vertical slice "A" in Fig. 1, *A* and *B* (sarcomere length, 2 .4 μm). In this slice the centroid of the first layer line is 432 Å, indicating that the main contribution in this region originates from the myosin-based helical structure. The intensity of the myosin-based layer line is significantly enhanced as ionic strength is lowered. The standard spacings (430, 385, and 365 Å) of the first myosin, troponin, and actin layer lines are indicated. (*B*) Same conditions as in (*A*), but at non-overlap sarcomere length, 4.1 μm. The effect of ionic strength is not evident, indicating that the enhancement in (*A*) is due to cross-bridge attachment. There are other layer lines in the diffraction patterns. The centroid of the layer line shown here is at ~389 Å. Most likely, the layer lines originate from the thin filaments because they are present at the similarly low intensity levels even under the conditions where the myosin filaments are disordered (e.g., under ATP-free condition (Xu et al., 1999b)). It is also possible that the disordered myosin population contributes a low residual level of intensity to the first myosin layer line. The profiles were first subtracted by fitted background curves.

TABLE 1 Changes in intensity ratios and spacings of the equatorial reflections from the NPM-reacted fiber bundles at high and low ionic strengths

	Before NPM	After NPM	
Conditions	5°C Relax (170 mM)	5°C Relax (170 mM)	5°C Relax (27 mM)
I_{11}/I_{10} ± SEM (*n*)	0.62 ± 0.05 (3)	0.74 ± 0.02 (7)	1.64 ± 0.01 (6)
d_{10} ± SEM (*n*) (Å)	424.5 ± 2.7 (3)	424.7 ± 1.5 (7)	399.9 ± 2.4 (6)
d_{11} ± SEM (*n*) (Å)	245.3 ± 0.8 (3)	244.8 ± 0.6 (7)	229.3 ± 0.9 (6)

I_{10} and I_{11} are the integrated intensities of [1, 0] and [1, 1] reflections, respectively. d_{10} is the lattice spacing of the [1, 0] plane; d_{11}, the [1, 1] plane.

head of the cross-bridge. For this reason, the intensity distributions in Fig. 7 were used for modeling (see the accompanying paper (Gu et al.).

Lack of contribution to the sixth (59 Å) actin layer line: a unique feature

Fig. 8 shows the intensity profiles along the 59 Å layer line shown in Fig. 1, *A* and *B*. The two profiles are statistically indistinguishable (Table 3). This is in sharp contrast to the diffraction patterns observed for strongly bound cross-bridges, e.g., in rigor (Huxley and Brown, 1967) or in activated muscle (Kraft et al., 1998; Tsaturyan et al., 1999), where the intensities of actin layer lines are predominant at the expense of the myosin layer lines and the distribution of the sixth actin layer line shifts toward the meridian. In addition, preliminary results indicate that upon formation of the A·M·ADP·P_i state, the intensity of the sixth layer line increases (Xu et al., 2001). Therefore, the lack of sensitivity reported here is a unique feature of the A·M·ATP state.

The meridional reflections

The intensities along the meridian obtained from NPM-treated muscle in relaxing solution at μ = 170 and 27 mM at 5°C are shown in Fig. 9. When the ionic strength is lowered, the integrated intensities of the myosin third meridional reflection, M_3, and the second, M_2, increase significantly, but the sixth, M_6, shows a relatively smaller increase (Table 4). The spacing of the centroid of M_3 (D_{M3}) is 144.6 Å and of M_6 (D_{M6}) is 72.4 Å. They remain the same, within experimental error, regardless of the ionic strength. These spacings differ significantly from untreated relaxed muscle at higher temperatures (>20°C) with D_{M3} = 143.4 Å and D_{M6} = 71.5 Å (Xu et al., 1997).

Experiments at non-overlap sarcomere length

Ionic strength could have a direct effect on the helical structures of the myofilaments independent of cross-bridge attachment. To test whether this was so, experiments on NPM-reacted muscle were also carried out at non-overlap sarcomere length to avoid any cross-bridge attachment. The muscle bundles were first over-stretched to 4.0–4.2 μm (see Xu et al., 1999b) and then treated with NPM the same way as for the full-overlap muscle bundles. There are layer lines present in the diffraction patterns. The centroid of the first layer line is at ~389 Å. Most likely, they originate from the thin filaments, because they are present (at similar intensity levels) even under conditions where the myosin filaments are disordered (e.g., under ATP-free condition (Xu et al., 1999b)). It is also possible that the disordered population may contribute a low residual level of intensity to the first myosin layer line. The present data also show that the patterns obtained at μ = 170 and 27 mM at 5°C are very similar (patterns not shown). In Fig. 5 *B* the profiles

TABLE 2 Integrated intensities and spacings of the first mixed myosin-actin layer line in the vertical slices A, B, C, and D

	Before NPM	After NPM	
Conditions	5°C Relax (170 mM)	5°C Relax (170 mM)	5°C Relax (27 mM)
I_A ± SEM (*n*)	0.45 ± 0.10 (3)	0.19 ± 0.02 (7)	0.45 ± 0.02 (6)
I_B ± SEM (*n*)	0.50 ± 0.08 (3)	0.23 ± 0.02 (7)	0.71 ± 0.06 (6)
I_C ± SEM (*n*)	0.63 ± 0.06 (3)	0.58 ± 0.05 (7)	1.49 ± 0.08 (6)
I_D ± SEM (*n*)	0.62 ± 0.09 (3)	0.71 ± 0.09 (7)	1.52 ± 0.18 (6)
d_A ± SEM (*n*) (Å)	432.2 ± 2.8 (3)	432.9 ± 2.0 (7)	432.0 ± 1.0 (6)
d_B ± SEM (*n*) (Å)	422.5 ± 3.9 (3)	401.9 ± 5.5 (7)	406.5 ± 1.8 (6)
d_C ± SEM (*n*) (Å)	394.2 ± 6.2 (3)	394.9 ± 4.0 (7)	398.9 ± 1.2 (6)
d_D ± SEM (*n*) (Å)	368.8 ± 23.4 (3)	377.8 ± 5.0 (7)	378.1 ± 2.5 (6)

The lateral widths of the vertical slices: "A," 0.00305–0.00390 $Å^{-1}$ (328 − 256 Å in real space); "B," 0.00404–0.00543 $Å^{-1}$ (248 − 184 Å); "C," 0.00610–0.00964 $Å^{-1}$ (164 − 104 Å); "D," 0.00978–0.01512 $Å^{-1}$ (102 − 66 Å). All integrated intensities (I) in the tables were normalized by the integrated intensity of the equatorial reflection [1, 0] obtained from the same NPM-treated bundles in the relaxing solution at μ = 50 mM and 5°C. The centroids refer to the slices "A," "B," "C," and "D." For example, "d_A" refers to the centroid of the entire intensity distribution in slice "A" from the overlapping layer lines in Fig. 1, *A* or *B*. "d_B," "d_C," and "d_D" are similarly defined.

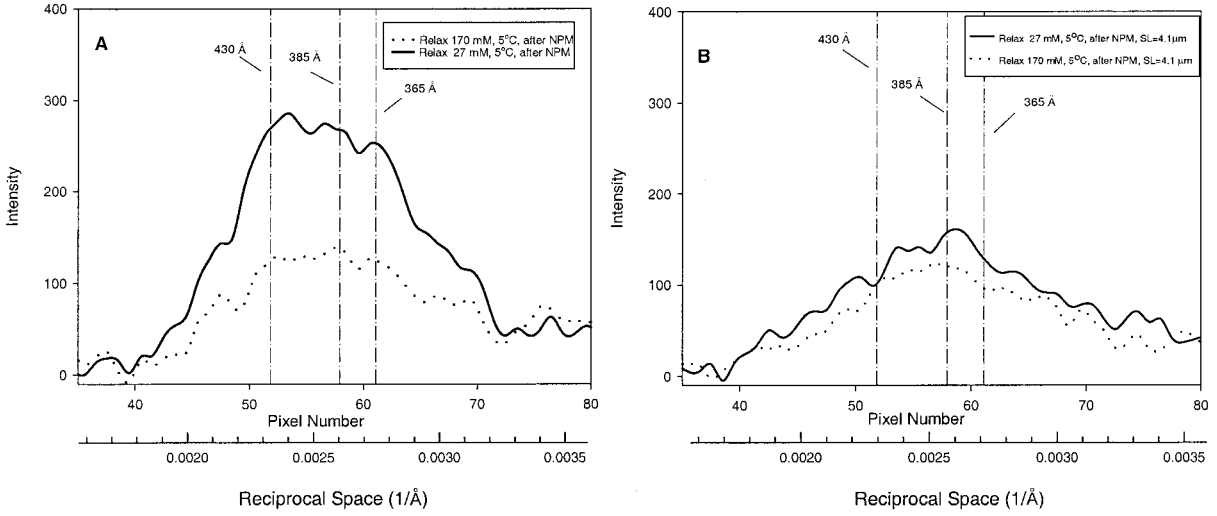

FIGURE 6 Effects of ionic strength on layer line intensities (II). The profiles only show the overlap region of the myosin-actin layer lines for clarity. *Solid lines*, μ = 27 mM; *dotted lines*, μ = 170 mM. (*A*) Data from slice "B" in Fig. 1, *A* and *B*. Sarcomere length, 2.4 μm. In this region, intensities of both the first myosin layer line at ~430 Å and the first actin layer line at ~365 Å are increased with increasing attachment. (*B*) Same conditions as in (*A*) except that sarcomere length = 4.1 μm. There is an increase (~15%) in total intensity with decreasing ionic strength. The magnitude of increase is much smaller than the increase observed in (*A*). Therefore, the overall increase in layer intensities in (*A*) cannot be simply explained by the direct effect of ionic strength. The profile lines were first subtracted by fitted background curves.

(based on slice A) obtained at the two ionic strengths are almost identical. In Fig. 6 *B* the profiles (based on slice B) show a slight increase (<15%) in the total integrated intensity when the ionic strength is lowered from 170 to 27 mM. The increase is considerably smaller than that observed at full overlap (Fig. 6 *A*). Considering the small effects observed in the diffraction patterns, these results provide a strong support that changes of ionic strength have little direct effect on the helix of the NPM-treated thick filaments.

DISCUSSION

The key features of the x-ray diffraction pattern due to weakly attached cross-bridges in the A·M·ATP state are 1) both the intensity of the myosin-based and the first actin-based layer lines are enhanced by attachment; and yet 2) the sixth actin layer line (at 59 Å) remains largely unchanged (Table 4). However, the intensities remain weak despite substantial attachment. In our previous study (Xu et al., 1997), only a shift of the centroid of the first layer line was observed, suggesting that the actin layer line was enhanced. The present study provides clear evidence for the enhancement. Furthermore, the origin of the enhancement is now exclusively attributed to the weak attachment in the A·M·ATP state. The result implies that there is added mass along the actin helix with a 37-nm repeat, further support that the binding site for this state is specific on actin. At first glance, the lack of change on the 5.9-nm layer line seems to be inconsistent with the idea of a site-specific binding on the actin filament, because the binding appears to add little to the genetic helix. However, modeling shows that the results can be explained by attachment at a site close to the N-terminus of actin with a wide range of orientations (Gu et al., 2002). Such attachment results in a combination of phases in the scattering functions that cancels contributions to the sixth layer line.

Another result to be noted is that the centroid of the third meridional reflection M_3 remains at 14.5 nm with the weak attachment (Table 4), indicating that in rabbit skeletal muscle the 14.5-nm spacing is not restricted to the strong binding states, e.g., in rigor (Huxley and Brown, 1967; Xu et al., 1997) and fully activated intact rabbit psoas (Losey and Yu, unpublished results). In fact, for the skinned rabbit psoas muscle fibers, only the intermediates with bound ADP·P_i (i.e., the M·ADP·P_i and A·M·ADP·P_i states), where the distribution of the cross-bridges is well ordered, showed the M_3 spacing being 14.3 nm (Xu et al., 1999b, 2001). All the other attached and detached states exhibited the M_3 spacing at ~14.5 nm.

It might be questioned whether the NPM-treated muscle fibers in the presence of MgATP behave as a structural analog of the untreated muscle in the A·M·ATP/M·ATP states. NPM is a monofunctional reagent with a single reactive maleimide ring, which under the conditions used here reacts specifically and alkylates fully both sulfhydryls (Cys-707 and Cys-697) in the myosin head (Xie et al., 1997). Although there are indications of some structural differences as revealed by differential scanning calorimetry between the unreacted and the NPM-reacted myosins in the presence of ATP analogs, e.g., ADP·AlF_4 (Bobkov and Reisler, 2000), the differences are probably undetectable at the resolution of the present study, as shown by their similar

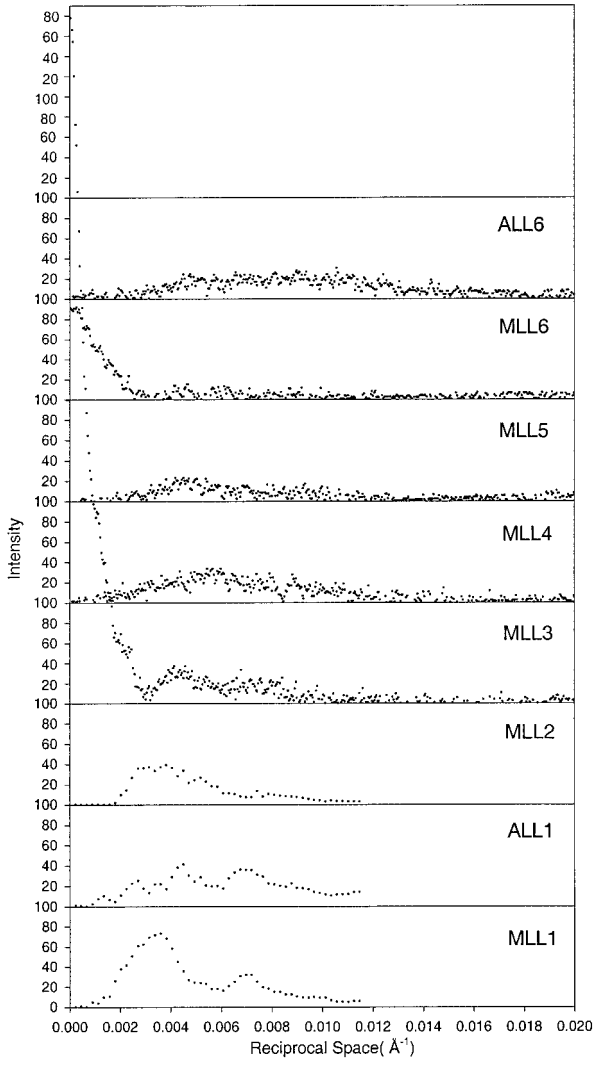

FIGURE 7 Intensity profiles along the myosin-based layer lines (MLL1-MLL6) and the actin-based layer lines (ALL1 and ALL6) of the x-ray diffraction pattern shown in Fig. 1 *A*. The layer lines for MLL1, ALL1, and MLL2 on the figure were reconstructed from the original data by curve-fitting contiguous vertical cuts (5 pixels wide) across the layer lines using Peak Fit (Jandel Scientific). The layer lines MLL3-MLL6 and ALL6 were obtained by the horizontal cuts along each layer line. All data shown here were first subtracted by curve-fitted scattering background. The intensity distributions in this figure were used for modeling (see the accompanying paper (Gu et al., 2002).

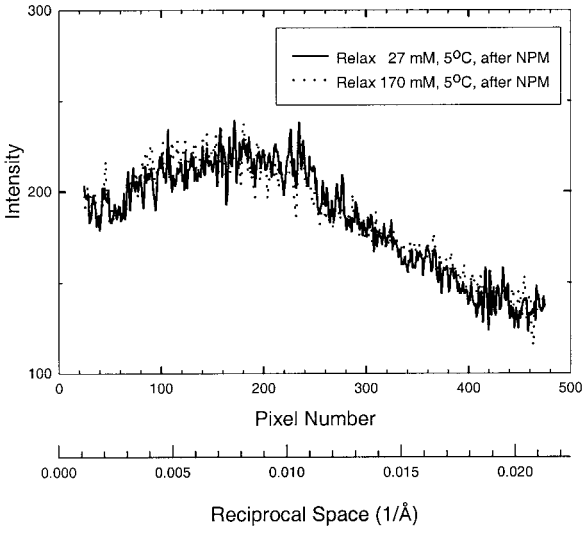

FIGURE 8 Intensity profiles along the sixth actin layer line at 59 Å of the patterns obtained from an NPM-reacted bundle in the relaxing solutions at 5°C, at μ = 27 mM (*solid line*) and at μ = 170 mM (*dotted line*). The sixth actin layer line is insensitive to the weak binding of the A·M·ATP state.

x-ray diffraction patterns (Xu et al., 1998; Fig. 2) and mechanical properties (Barnett et al., 1992). Another indication of the structural analog is that the x-ray diffraction patterns of the NPM-reacted fibers are very similar to those obtained in the presence of the slowly hydrolyzable nucleotide ATPγS. For myosin with bound ATPγS, the equilibrium is mainly in the unhydrolyzed state (Goody and Eckstein, 1971). Although the ATPγS study was not as extensive, it was shown that in the presence of saturating ATPγS at μ = 80 mM and 1°C, the first layer line in the diffraction patterns also consisted of a mixture of myosin and actin-based layer lines (Kraft et al., 1999).

The increase in the fraction of weakly bound cross-bridges was induced by lowering the ionic strength. It could be that the change in intensities was due to improved lattice order. However, the changes observed at out-of-overlap sarcomere length were much smaller than those at full overlap (Figs. 5 *B* and 6 *B*). Therefore, the increase in layer line intensities could not simply be explained by lattice ordering or some direct ionic effects. Rather, it appears that the cross-bridges with bound ATP while not attached to actin are flexible, fluctuating incoherently with large amplitudes in all three dimensions in the filament lattice, exhibiting a high degree of disorder (Xu et al., 1999b). Once they are attached to actin, even though weakly, the amplitude of fluctuation is reduced and the disorder is decreased. The helical packing of the myosin molecules in the thick filament is thus more clearly revealed, exhibiting the myosin based layer lines. The result underscores the novel and unexpected property of the A·M·ATP state that despite its low affinity, it nevertheless stabilizes the filaments.

It should be mentioned that there appears to be a significant fraction of cross-bridges making non-stereospecific contacts with actin and not generating force at low temperature (Tsaturyan et al., 1999). Such weakly bound cross-bridges appear to differ from the present study in that they make no contribution to the actin layer lines until converted to the force-generating state by temperature-jump.

Modeling (Gu et al., 2002) based on the present data suggests a wide range of attachment angles and substantial deviations at the S1-S2 junction from the lattice points.

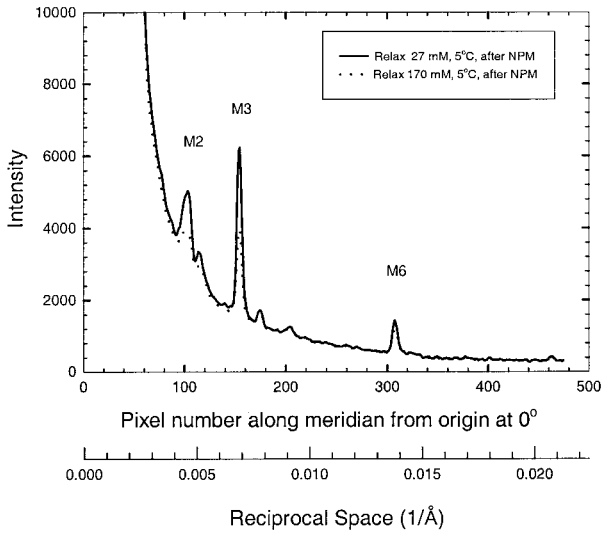

FIGURE 9 Intensity profiles along the meridian of the patterns (Fig. 1, *A* and *B*) obtained from an NPM-reacted bundle in the relaxing solutions at 5°C, at μ = 27 mM (*solid line*) and at μ = 170 mM (*dotted line*). The spacing of the third meridional reflection remains at 14.5 nm regardless of attachment. The intensities and the spacings of the meridional reflections are listed in Table 4.

However, even without the modeling one may conclude that there is considerable disorder in the distribution of myosin heads and perturbation in the helical order of the myosin filament because the intensities of the myosin layer lines remain weak, despite a large fraction of cross-bridges attached. Such flexibility exhibited by the weak binding states M·ATP ↔ A·M·ATP, we believe, entails their significance in the process of force generation. It has been shown that in solution, the affinity M·ADP·P_i for actin is low (White et al., 1997). In fibers the probability for attaching to actin is further reduced because the myosin heads in the M·ADP·P_i state are distributed in a well-ordered helical array (Xu et al., 1999b) and appear to "wrap around" the myosin filament backbone, away from the actin filament surface (Malinchik et al., 1997). Preliminary data suggest that even the few cross-bridges bound in the A·M·ADP·P_i state also appear to be well ordered (Xu et al., 2001). Therefore, some degree of disorder is necessary to improve the probability of attachment. The flexible actomyosin complex (M·ATP ↔ A·M·ATP) could well fulfill such a requirement, making the attached states (bottom of Scheme 1) the dominant pathway in the cross-bridge cycle. This idea is consistent with the close correlation between the rate-limiting step of the steady-state hydrolysis of nucleoside triphosphates by actomyosin-S1 in solution and the steady-state hydrolysis by isometrically contracting muscle fibers (White et al., 1993; Pate et al., 1993). A similar observation on the correlation between ATPase in solution and the rate of force redevelopment in fibers was also reported by Brenner and Eisenberg (1986).

However, in the relaxed muscle under physiological conditions, ~10% of the cross-bridges are attached to actin (Kraft et al., 1995). The rest is mostly distributed in the M·ADP·P_i state (Xu et al., 1999b). At first glance, the activation process through the M·ATP ↔ A·M·ATP pathway appears untenable. However, the rate constants for the hydrolysis M·ATP ↔ M·ADP·P_i are fast (Taylor, 1977) and the states are in reversible equilibrium. As an increasing fraction of A·M·ATP proceeds to the force-producing states, because of its fast kinetics, a redistribution of populations, e.g., M·ADP·P_i → M·ATP → A·M·ATP among the equilibrium states can occur rapidly and is therefore highly feasible.

In relaxed frog skeletal muscle, although weakly attached cross-bridges have also been observed by x-ray diffraction (Xu et al., 1987), the equilibrium population of A·M·ATP, even at low temperature and low ionic strength, is ~15%. In flat fish muscle, few weak binding cross-bridges were detected (Squire et al., 1991). However, the kinetics of the actomyosin interactions found in these muscles is fast compared to the rabbit muscle. The fast kinetics could well compensate for the small population in the M·ATP → A·M·ATP equilibrium. Furthermore, in intact frog muscle, it was shown (Huxley et al., 1982) that the restoration of the myosin layer lines lagged by ~15 ms following muscle relaxation, which would correspond with the time expected for hydrolysis of bound ATP. However, it is possible that there is a population of disordered M·ADP·P_i cross-bridges. The existence of such a state has not yet been determined.

It has been shown that skeletal myosin filament becomes disordered following the phosphorylation of the myosin regulatory light chain (Levine et al., 1995, 1996) at submaximal level of calcium. The force level and redevelopment kinetics were enhanced. Cardiac muscle fibers appear to exhibit similar behavior (Levine et al., 2001). Phosphorylation of the myosin light chain could be a complementary

TABLE 3 Integrated intensities and spacings of the sixth actin layer line at 59 Å

	Before NPM	After NPM	
Conditions	5°C Relax (170 mM)	5°C Relax (170 mM)	5°C Relax (27 mM)
I_{59} ± SEM (*n*)	2.97 ± 0.56 (3)	3.05 ± 0.09 (7)	3.43 ± 0.13 (6)
d_{59} ± SEM (*n*) (Å)	59.2 ± 0.1 (3)	59.0 ± 0.1 (7)	59.1 ± 0.1 (6)

Definitions for intensities and centroid spacings are the same as in Table 2.

TABLE 4 Integrated intensities and spacings of the third and sixth myosin reflections on the meridian

	Before NPM	After NPM	
Conditions	5°C Relax (170 mM)	5°C Relax (170 mM)	5°C Relax (27 mM)
$I_{M3} \pm$ SEM (n)	2.55 ± 0.39 (3)	3.67 ± 0.12 (7)	6.32 ± 0.19 (6)
$d_{M3} \pm$ SEM (n) (Å)	144.6 ± 0.3 (3)	144.8 ± 0.1 (7)	144.6 ± 0.1 (6)
$I_{M6} \pm$ SEM (n)	0.91 ± 0.15 (3)	1.18 ± 0.06 (7)	1.58 ± 0.06 (6)
$d_{M6} \pm$ SEM (n) (Å)	72.3 ± 0.1 (3)	72.4 ± 0.1 (7)	72.4 ± 0.1 (6)

Normalized intensities of the third and the sixth myosin meridional reflections. Definitions for intensities and centroid spacings are the same as in Table 2.

mechanism of disordering the myosin filament. The biochemical state of the phosphorylated myosin is not yet clear, and the potentiation appears effective at the submaximal calcium level.

In summary, the present study together with our previous studies has provided a fuller structural characterization of the cross-bridge ATPase cycle. With the present study of the A·M·ATP state, seven of the eight major intermediate biochemical states of the cross-bridge hydrolysis cycle in muscle fibers have been described in detail. Experiments are in progress to determine the conformation of the actomyosin complex in the key intermediate A·M·ADP·P_i. With the completion of the characterizations of the intermediate states, together with atomic structures, a picture of the structural basis of contraction should emerge.

The authors thank Dr. Gerald Offer for his critical reading of the manuscript. The authors also thank the staff of Beamlines X9B and X27C at the National Synchrotron Light Source (NSLS) for their expert assistance.

REFERENCES

Barnett, V. A., A. Ehrlich, and M. Schoenberg. 1992. Formation of ATP-insensitive weakly binding crossbridges in single rabbit psoas fibers by treatment with phenylmaleimide or para-phenylenedimaleimide. *Biophys. J.* 61:358–367.

Barnett, V. A., and M. Schoenberg. 1993. The strength of binding of the weakly binding crossbridge created by sulfhydryl modification has very low calcium sensitivity. *Adv. Exp. Med. Biol.* 332:133–138.

Bobkov, A., and E. Reisler. 2000. Is SH1-SH-cross-linked myosin subfragment 1 a structural analog of the weakly bound state of myosin? *Biophys. J.* 79:460–467.

Brenner, B. 1986. The cross-bridge cycle in muscle. Mechanical, biochemical, and structural studies on single skinned rabbit psoas fibers to characterize cross-bridge kinetics in muscle for correlation with the actomyosin-ATPase in solution. *Basic Res. Cardiol.* 81:1–15.

Brenner, B., and E. Eisenberg. 1986. The rate of force generation in muscle: correlation with actomyosin ATPase in solution. *Proc. Natl. Acad. Sci. U.S.A.* 83:3542–3546.

Brenner, B., M. Schoenberg, J. M. Chalovich, L. E. Greene, and E. Eisenberg. 1982. Evidence for cross-bridge attachment in relaxed muscle at low ionic strength. *Proc. Natl. Acad. Sci. U.S.A.* 79:7288–7291.

Brenner, B., and L. C. Yu. 1985. Equatorial x-ray diffraction from single skinned rabbit psoas fibers during various degrees of activation. Changes in intensities and lattice spacing. *Biophys. J.* 48:829–834.

Brenner, B., L. C. Yu, and J. M. Chalovich. 1991. Parallel inhibition of active force and relaxed fiber stiffness in skeletal muscle by caldesmon: implications for the pathway to force generation. *Proc. Natl. Acad. Sci. U.S.A.* 88:5739–5743.

Brenner, B., L. C. Yu, L. E. Greene, E. Eisenberg, and M. Schoenberg. 1986. Ca^{2+}-sensitive cross-bridge dissociation in the presence of magnesium pyrophosphate in skinned rabbit psoas fibers. *Biophys. J.* 50: 1101–1108.

Brenner, B., L. C. Yu, and R. J. Podolsky. 1984. X-ray diffraction evidence for cross-bridge formation in relaxed muscle fibers at various ionic strengths. *Biophys. J.* 46:299–306.

Chalovich, J. M. 1992. Actin mediated regulation of muscle contraction. *Pharmacol. Ther.* 55:95–148.

Chalovich, J. M., L. E. Greene, and E. Eisenberg. 1983. Crosslinked myosin subfragment 1: a stable analogue of the subfragment-1-ATP complex. *Proc. Natl. Acad. Sci. U.S.A.* 80:4909–4913.

Ehrlich, A., V. A. Barnett, H. C. Chen, and M. Schoenberg. 1995. The site and stoichiometry of the *N*-phenylmaleimide reaction with myosin when weakly binding crossbridges are formed in skinned rabbit psoas fibers. *Biochim. Biophys. Acta.* 1232:13–20.

Eisenberg, E., and T. L. Hill. 1985. Muscle contraction and free energy transduction in biological systems. *Science* (Wash. DC). 227:999–1006.

Fisher, A. J., C. A. Smith, J. Thoden, R. Smith, K. Sutoh, H. M. Holden, and I. Rayment. 1995. Structural studies of myosin:nucleotide complexes: a revised model for the molecular basis of muscle contraction. *Biophys. J.* 68:19S–26S.

Frisbie, S. M., S. Xu, J. M. Chalovich, and L. C. Yu. 1998. Characterizations of cross-bridges in the presence of saturating concentrations of MgAMP-PNP in rabbit permeabilized psoas muscle. *Biophys. J.* 74: 3072–3082.

Geeves, M. A., and K. C. Holmes. 1999. Structural mechanism of muscle contraction. *Annu. Rev. Biochem.* 68:687–728.

Goody, R. S., and F. Eckstein. 1971. Thiophosphate analogs of nucleoside di- and triphosphates. *J. Am. Chem. Soc.* 93:6252.

Gu, J., S. Xu, and L. C. Yu. 2002. A model of cross-bridge attachment to actin in the AMATP state based on x-ray diffraction from permeabilized rabbit psoas muscle. *Biophys. J.* 82:2123–2133.

Houdusse, A., A. G. Szent-Gyorgyi, and C. Cohen. 2000. Three conformational states of scallop myosin S1. *Proc. Natl. Acad. Sci. U.S.A.* 97:11238–11243.

Huxley, H. E., and W. Brown. 1967. The low-angle x-ray diagram of vertebrate striated muscle and its behaviour during contraction and rigor. *J. Mol. Biol.* 30:383–434.

Huxley, H. E., A. F. Faruqi, M. Kress, J. Bordas, and M. H. J. Koch. 1982. Time-resolved x-ray diffraction studies of the myosin layer-line reflections during muscle contraction. *J. Mol. Biol.* 158:637–684.

Juanhuix, J., J. Bordas, J. Campmany, A. Svensson, M. L. Bassford, and T. Narayanan. 2001. Axial disposition of myosin heads in isometrically contracting muscles. *Biophys. J.* 80:1429–1441.

Kim, D. S., Y. Takezawa, M. Ogino, T. Kobayashi, T. Arata, and K. Wakabayashi. 1998. X-ray diffraction studies on the structural changes of rigor muscles induced by binding of phosphate analogs in the presence of MgADP. *Biophys. Chem.* 74:71–82.

Kraft, T., J. M. Chalovich, L. C. Yu, and B. Brenner. 1995. Parallel inhibition of active force and relaxed fiber stiffness by caldesmon fragments at physiological ionic strength and temperature conditions: additional evidence that weak cross-bridge binding to actin is an essential intermediate for force generation. *Biophys. J.* 68:2404–2418.

Kraft, T., T. Mattei, and B. Brenner. 1998. Structural features of force-generating cross-bridges. A 2D-x-ray diffraction study. *Adv. Exp. Med. Biol.* 453:289–295.

Kraft, T., S. Xu, B. Brenner, and L. C. Yu. 1999. The effect of thin filament activation on the attachment of weak binding cross-bridges: a two-dimensional x-ray diffraction study on single muscle fibers. *Biophys. J.* 76:1494–1513.

Levine, R. J., R. W. Kensler, Z. Yang, J. T. Stull, and H. L. Sweeney. 1996. Myosin light chain phosphorylation affects the structure of rabbit skeletal muscle thick filaments. *Biophys. J.* 71:898–907.

Levine, R. J., R. W. Kensler, Z. Yang, and H. L. Sweeney. 1995. Myosin regulatory light chain phosphorylation and the production of functionally significant changes in myosin head arrangement on striated muscle thick filaments. *Biophys. J.* 68:224.

Levine, R., A. Weisberg, I. Kulikovskaya, G. McClellan, and S. Winegrad. 2001. Multiple structures of thick filaments in resting cardiac muscle and their influence on cross bridge interactions. *Biophys. J.* 81:1070–1082.

Malinchik, S., S. Xu, and L. C. Yu. 1997. Temperature-induced structural changes in the myosin thick filament of skinned rabbit psoas muscle. *Biophys. J.* 73:2304–2312.

McKenna, N. M., Y. Wang, and M. E. Konkel. 1989. Formation and movement of myosin-containing structures in living fibroblasts. *J. Cell Biol.* 109:1163–1172.

Milligan, R. A., M. Whittaker, and D. Safer. 1990. Molecular structure of F-actin and location of surface binding sites. *Nature (Lond.).* 348: 217–221.

Papp, S., D. Eden, and S. Highsmith. 1992. Nucleotide- and temperature-induced changes in myosin subfragment-1 structure. *Biochim. Biophys. Acta.* 1159:267–273.

Pate, E., K. Franks-Skiba, H. White, and R. Cooke. 1993. The use of differing nucleotides to investigate cross-bridge kinetics. *J. Biol. Chem.* 268:10046–10053.

Rayment, I., H. Holden, M. Whittaker, C. Yohn, M. Lorenz, K. Holmes, and R. Milligan. 1993a. Structure of the actin-myosin complex and its implications for muscle contraction. *Science (Wash. DC).* 261:59–65.

Rayment, I., W. Rypniewski, K. Schmidt-Base, R. Smith, D. R. Tomchick, M. M. Benning, D. A. Winkelmann, G. Wesenberg, and H. M. Holden. 1993b. Three-dimensional structure of myosin subfragment-1: a molecular motor. *Science (Wash. DC).* 261:50–58.

Rayment, I., C. Smith, and R. G. Yount. 1996. The active site of myosin. *Annu. Rev. Physiol.* 58:671–702.

Schroder, R. R., D. J. Manstein, W. Jahn, H. Holden, I. Rayment, K. C. Holmes, and J. A. Spudich. 1993. Three-dimensional atomic model of F-actin decorated with Dictyostelium myosin S1. *Nature (Lond.).* 364: 171–174.

She, M., J. Gu, S. Xu, J. M. Chalovich, and L. C. Yu. 1999. X-ray diffraction study of skeletal muscle labeled with troponin-T antibody. *Biophys. J.* 76:32*a.* (Abstr.).

Shih, W. M., Z. Gryczynski, J. R. Lakowicz, and J. Spudich. 2000. A FRET-based sensor reveals large ATP hydrolysis-induced conformation changes and three distinct states of the molecular motor myosin. *Cell.* 102:683–694.

Squire, J. M., R. J. Podolsky, J. S. Barry, L. C. Yu, and B. Brenner. 1991. X-ray diffraction testing for weak-binding crossbridges in relaxed bony fish muscle fibres at low ionic strength. *J. Struct. Biol.* 107:221–226.

Taylor, E. W. 1977. Transient phase of adenosine triphosphate hydrolysis by myosin, heavy meromyosin, and subfragment 1. *Biochemistry.* 16: 732–739.

Taylor, E. W. 1989. Actomyosin ATPase mechanism and muscle contraction. *Prog. Clin. Biol. Res.* 315:9–14.

Tsaturyan, A. K., S. Y. Bershitsky, R. Burns, and M. A. Ferenczi. 1999. Structural changes in the actin-myosin cross-bridges associated with force generation induced by temperature jump in permeabilized frog muscle fibers. *Biophys. J.* 77:354–372.

Wakabayashi, T., T. Akiba, K. Hirose, A. Tomioka, M. Tokunaga, C. Suzuki, C. Toyoshima, K. Sutoh, K. Yamamoto, T. Matsumoto, K. Sacki, and Y. Amemiya. 1988. Temperature induced changes of thick filament and location of the functional site of myosin. *In* Molecular Mechanism of Muscle Contraction. H. Sugi and G. H. Pollack, editors. Plenum Publishing Co., New York. 39–48.

White, H. D., B. Belknap, and W. Jiang. 1993. Kinetics of binding and hydrolysis of a series of nucleoside triphosphates by actomyosin-S1. Relationship between solution rate constants and properties of muscle fibers. *J. Biol. Chem.* 268:10039–10045.

White, H., B. Belknap, and M. R. Webb. 1997. Kinetics of nucleoside triphosphate cleavage and phosphate release steps by associated rabbit skeletal actomyosin, measured using a novel fluorescent probe for phosphate. *Biochemistry.* 36:11828–11836.

Whittaker, M., E. M. Wilson-Kubalek, J. E. Smith, L. Faust, R. A. Milligan, and H. L. Sweeney. 1995. A 35-A movement of smooth muscle myosin on ADP release. *Nature (Lond.).* 378:748–751.

Wray, J. 1987. Structure of relaxed myosin filaments in relation to nucleotide state in vertebrate skeletal muscle. *J. Mus. Res. Cell. Motil.* 8:62a.

Xiao, M., H. Li, G. E. Snyder, R. Cooke, R. G. Yount, and P. R. Selvin. 1998. Conformational changes between the active-site and regulatory light chain of myosin as determined by luminescence resonance energy transfer: the effect of nucleotides and actin. *Proc. Natl. Acad. Sci. U.S.A.* 95:15309–15314.

Xie, L., W. X. Li, V. A. Barnett, and M. Schoenberg. 1997. Graphical evaluation of alkylation of myosin's SH1 and SH2: the *N*-phenylmaleimide reaction. *Biophys. J.* 72:858–865.

Xie, L., W. X. Li, T. Rhodes, H. White, and M. Schoenberg. 1999. Transient kinetic analysis of *N*-phenylmaleimide-reacted myosin subfragment-1. *Biochemistry.* 38:5925–5931.

Xu, S., J. Gu, G. Melvin, and L. C. Yu. 2001. Evidence that the conformation of the actomyosin complex with bound ADP·Pi (the A·M·ADP·Pi state) differs from that in the A·M·ATP state. *Biophys. J.* 80:267*a.* (Abstr.).

Xu, S., J. Gu, T. Rhodes, B. Belknap, G. Rosenbaum, G. Offer, H. White, and L. C. Yu. 1999b. The M·ADP·P_i state is required for helical order in the thick filaments of skeletal muscle. *Biophys. J.* 77:2665–2676.

Xu, S., J. Gu, and L. C. Yu. 1999a. Characterizing and modeling the structure of weakly attached cross-bridges in the A·M·ATP state in skinned rabbit psoas muscle. *Biophys. J.* 76:33*a.* (Abstr.).

Xu, S., M. Kress, and H. E. Huxley. 1987. X-ray diffraction studies of the structural state of crossbridges in skinned frog sartorius muscle at low ionic strength. *J. Muscle Res. Cell Motil.* 8:39–54.

Xu, S., S. Malinchik, T. Kraft, B. Brenner, and L. C. Yu. 1996. X-ray diffraction evidence that attachment conformation of weakly bound crossbridges in muscle is highly variable (nonstereospecific). *Biophys. J.* 70:290*a*. (Abstr.).

Xu, S., S. Malinchik, Th. Kraft, B. Brenner, and L. C. Yu. 1997. X-ray diffraction studies of cross-bridges weakly bound to actin in relaxed skinned fibers of rabbit psoas muscle. *Biophys. J.* 73:2655–2666.

Xu, S., L. C. Yu, and M. Schoenberg. 1998. Behavior of *N*-phenylmaleimide-reacted muscle fibers in magnesium-free rigor solution. *Biophys. J.* 74:1110–1114.